Microstructure Evolution during Radiation Damage with Collision Cascades

Sci. Rep. RITU A40 (1994) pp. 29-47
No. 1, July 1994

Microstructure Evolution during Radiation Damage with Collision Cascades

M. Kiritani
Department of Nuclear Engineering, School of Engineering, Nagoya University
Furo-cho, Chikusa-ku, Nagoya 464, Japan

(Receied February 21, 1994)

Progress of the research on microstructural evolution during radiation damage accompanied with collision cascades, particularly by neutrons, is summarized from the research papers published since 1992. The major part of irradiation was performed with JMTR (Japan Materials Testing Reactor), and comparisons were made with the result of D-T fusion neutron irradiation with RTNS-II (Rotating Target Neutron Source, LLNL). The subjects concerned are: (1) Correlation of high-energy particle irradiation by use of the recoil energy spectrum, (2) Cascade localization induced bias effect for void growth, (3) Influence of primary recoil energy spectrum on microstructural evolution, (4) Variation of the cascade localization induced bias effect with material parameters and irradiation conditions, (5) Fluctuation effect of point defect reaction on nucleation of interstitial clusters, (6) Binary collision calculation of subcascade structure and its correspondence to observed subcascade defects in 14 MeV neutron irradiated copper, (7) Detection of the role of free point defects from the variation of defect structures near permanent sinks, (8) Low dose fission neutron irradiation on P- and Ti-modified austenitic alloys with improved temperature control, (9) Role of free point defects in defect structure evolution during cascade damage, (10) Origin of unbalanced reaction of vacancies and interstitial during irradiation with cascades and influence on microstructural evolution, (11) Influence of details of reactor history on microstructural development, (12) Exposure time and recoil energy dependence of defect accumulation, (13) Development of controlled temperature-cycle irradiation technique in JMTR, (14) Microstructure evolution by neutron irradiation during cyclic temperature variation, (15) Role of solute atoms on microstructural evolution in neutron irradiated nickel, (16) Microstructural evolution in low dose neutron irradiated Fe-15Ni-15Cr alloy, and (17) Effect of cascade localization induced bias effect and fluctuation of point defect reactions on defect structure evolution near planar sinks.

KEYWORDS: neutron radiation damage, fusion reactor materials, fusion neutron, reactor irradiation, cascade collision, microstructure, interstitial atom, lattice vacancy

1. Introduction

Post-irradiation experiment at the Oarai Branch, The Research Institute for Iron, Steel and Other Metals, Tohoku University, on materials irradiated with the Rotating Target Neutron Source (RTNS-II) at Lowrence Livermore National Laboratory in USA started in 1983.[1] Irradiation with RTNS-II finished in 1987, but the research is still in progress. During the course of progress of the research on fusion-neutron irradiated materials, the necessity of the improvement of the fission-reactor neutron irradiation became aware of.[2] After several years of efforts by related experimenters and engineers, an advanced technique to perform neutron irradiation in JMTR was established, with which the temperature can be controlled without being influenced by the operation mode of the reactor. The first comparison of the results of improved control with those of conventional control[3] was far enough to persuade the world wide researchers the necessity of the improvement.[4]

After establishing the advanced technique in the reactor irradiation, the improved control of temperature became to be regarded as common, though it had been regarded very special before. The technique to control the temperature not influenced by the reactor power enabled to design an arbitrary history of temperature during irradiation, and one typical application is found in the temperature-cycle irradiation which have been performed several times during these two years.[5] The irradiation technique with JMTR is now extending to design an irradiation rig called Multi-Division Removable Rig, with which parts of samples can be pulled one-by-one out from the irradiation field during the operation of the reactor.[6] These performances of research based on the Oarai Branch have been highly appreciated world wide. For example in the International Conference on Fusion Reactor Materials (ICFRM), the experimenters at the Oarai Branch are the only groups who have made continuous contribution by presenting invited papers.[7-11]

In this paper, the summarized report is made on the progress of research during the years of 1992 and 1993, limiting the subjects to those which are directly carried out at the Oarai Branch and at least to those which are based on the result from the work at Oarai. The present research group is performing irradiations with other particles than neutrons, such as electron irradiation with high voltage electron microscopes[12] and ion irradiations with accelerators,[13,14] but they are not included here, though the research content is closely related to the neutron irradiation. The accumulation of research results in this paper is done by the collaboration of many researchers. The number of collaborators are so large that it is difficult to list all of them as co-authors, and they can be refereed in the references of each part. Here at the beginning of the paper, the author acknowledge their continued collaboration.

2. Correlation of High-Energy Particle Irradiation by Use of the Recoil Energy Spectrum[15]

Characteristics of cascade damage both in collision processes and in defect processes followed after the collision are extracted, and discussions are given on their variation with primary recoil energy.

2.1. Recoil energy spectrum with a variety of energetic particles

Primary recoil energy spectra are compared for irradiations with representative energetic particles; electrons,

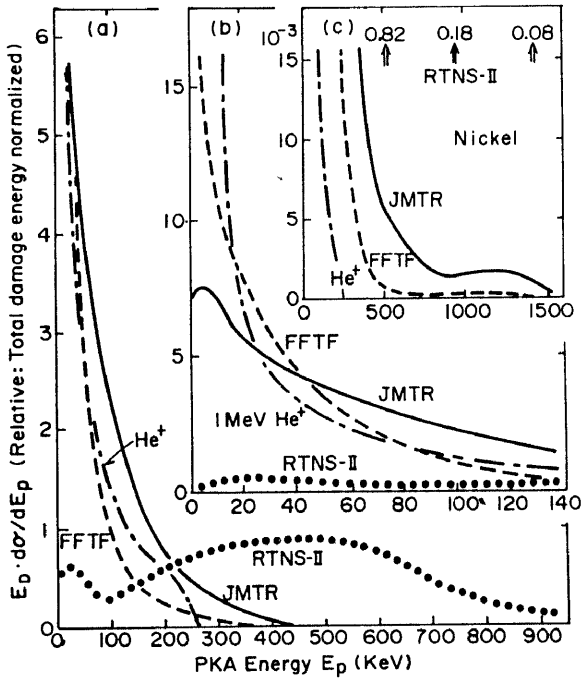

Fig. 1. Comparison of damage energy spectrum plotted against primary recoil energy for four energetic particle irradiations.

ions, fission and fusion neutrons. In Fig. 1, the damage energy deposited by the primary recoils (the product of the cross-section and the damage energy by a primary recoil) is plotted. RTNS-II (Rotating Target Neutron Source, LLNL) is an accelerator type D-T neutron source, JMTR (Japan Materials Testing Reactor, JAERI) is a 50 MW light-water reactor, and FFTF (Fast Flux Test Facility, HEDL) is a 200 MW fast breeder reactor. In this figure, the integrated area was normalized to be equal for all in order to compare the relative importance of the small and large recoils.

Prominent differences observed in the damage energy spectrum by the irradiation with different particles are briefly summarized. The recoil spectrum for 14 MeV neutrons in (a) has a large extended peak at higher energy recoil in contrast to the other three in which the energy decreases monotonically towards the high energy. The difference between JMTR and FFTF is worth noting. The population of large energy recoils in (c) is higher in the JMTR than in the FFTF, and the small energy recoil is more in FFTF than in JMTR in (b). This is contradictory to the common sense reasoning of fast neutrons in FFTF and thermal neutrons in JMTR. However, one should realize that this difference comes from the difference in the neutron energy spectrum at medium and high energies.

2.2. Formation of vacancy clusters from cascades

Correlation of the electron-microscopically-observed microstructures to the primary recoil energy spectrum has been done for 14 MeV-neutron-irradiated materials to determine the recoil energy dependence of the cascade damage structure. A summarizing example of the recoil energy dependence of cascade zone size is shown in Fig. 2. As for subcascades, assuming that vacancy clusters that appeared as closely spaced groups are formed from one single primary recoil, the larger number of groups was assigned to larger recoil energies in the same manner as in the analysis of cascade size. Examples are shown in Fig. 3.

The combination of the high density energy deposition in cascades derived from recoil energy spectrum analysis and the manner of progress of vacancy cluster formation is now shedding light on the underlying mechanism. The estimated deposited energy density in a large cascade is sufficient to raise the local temperature up to several tens of times the melting temperature. On the other hand, the number of observable vacancy clusters at very low fluence is much lower than the extrapolation from high fluence of a proportional increase with irradiation dose as shown in Fig. 4. From the irradiation dose of the transition from a square relation to a simple proportion, the volume of influence from one cascade could be estimated to be several times the volume of one cascade zone.

2.3. Formation of interstitial clusters and reaction of freely migrating point defects

Nucleation of interstitial clusters is confirmed to be performed by cascades. The formation of interstitial clusters by JMTR neutron irradiation occurs by three or more orders of magnitude weaker irradiation than the limit expected from the homogeneous introduction of point defects by electron irradiation. It can easily be concluded that the nucleation of interstitial clusters in neutron irradiation is carried out by localized interstitials at cascades.

A method to evaluate the amount of freely migrating point defects from interstitial loop growth is proposed. The annihilation speed of point defects to specimen surface sinks, which is the product of three terms, the jump

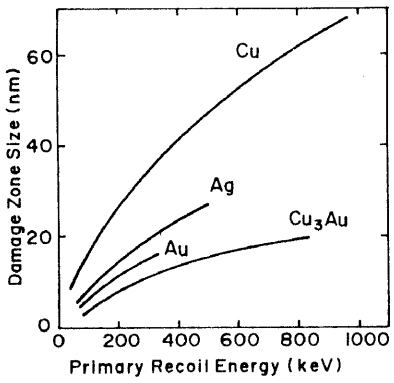

Fig. 2. Variation of the cascade zone size with the primary recoil energy in three materials.

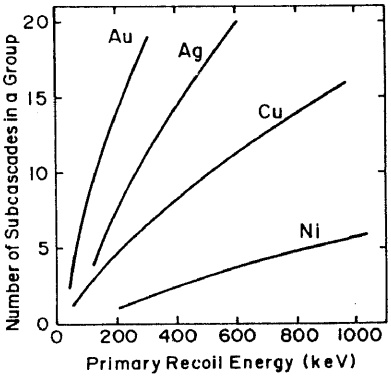

Fig. 3. Variation of the number of subcascades in a group with the primary recoil energy for four kind of metals.

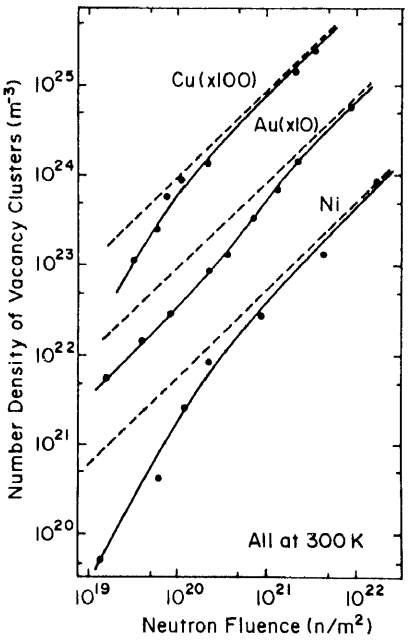

Fig. 4. Variation of the number of vacancy clusters at low dose in three kinds of fcc metals irradiated as thin foils at 300 K by 14 MeV neutrons.

frequency M, concentration C and the sink efficiency C_S, will be in equilibrium with the point defect production rate P:

$$C_S M C = P. \quad (1)$$

The growth rate of a loop of diameter L is

$$dL/dt = 2a Z_{IL} M_I C_I - 2a Z M_V C_V$$
$$= 2a \beta P/C_S, \quad (2)$$

where a is the increase of the loop radius by the absorption of an interstitial to each of all the sites around the loop and ß is the difference between the absorption cross-section of interstitials Z_{IL} and vacancies Z_{VL} at a site on the loop dislocation. In order to compare electron and neutron irradiation results directly, the ratio of equation 2 becomes

$$(dL/dt)_n/(dL/dt)_e = P_n/P_e, \quad (3)$$

when the observation and/or experiments are performed on specimens of the same thickness ($C_{sn} = C_{se}$). An advantage of this method is in the elimination of unknown parameters,

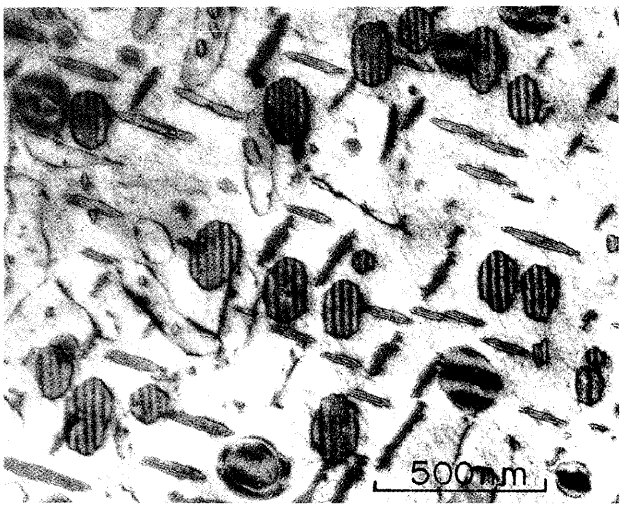

Fig. 5. Well developed dislocation loops of interstitial type in fission reactor irradiated Ni-2at.%Si. $1.0x10^{24}$n/m^2 (>1.0 MeV) at 673 K.

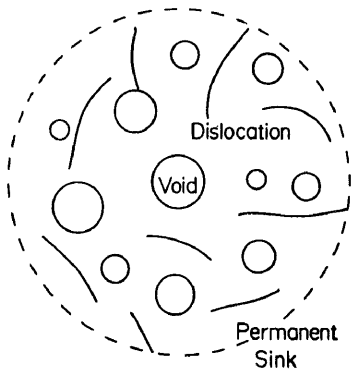

Fig. 6. Schematic illustration of voids and dislocations surrounded by a neutral permanent sink.

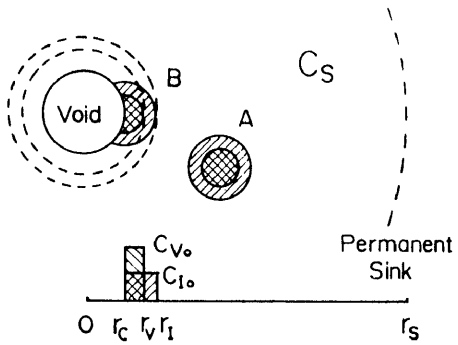

Fig. 7. Schematic illustration of a void with sink strength Cs used in the calculation. A and B are examples of cascades. The lower figure depicts the symbols used in the calculation.

such as Z, during the analysis. By use of old date on high temperature electron irradiated nickel, the growth speed of 0.10 nm/s under irradiation with 2 MeV electrons of $1.2x10^{23}$e/m^{2}s, which correspond to $1.2x10^{-3}$dpa/s, is compared with a JMTR irradiation up to 20 DEPA/atom for an irradiation time of 20 days in Fig. 5. The production rate Pn is found to be comparable to the point defect production by use of more than half of damage energy. This estimate of high efficiency in producing freely migrating point defects in fission reactor irradiated nickel has a clear contrast to the low efficiency in the case of 14 MeV neutrons.

3. Cascade Localization Induced Bias Effect for Void Growth[16]

The basic formulation of the cascade localization induced bias (CLIB) effect, which originates from the difference in the initial distribution of interstitials and vacancies in a cascade, is given and a theoretical method to evaluate the strength of the effect is developed. Figure 6 shows the general circumstances for the analysis, and Fig. 7 illustrates the model for the analysis.

Solutions for the dissipation of point defects produced by cascades are derived for three cases, and the growth of voids by CLIB is predicted. In Fig. 8 the calculated average void swelling rate is shown as a function of the distance from the surrounding permanent sink. In the case of only one void at the center of a spherical permanent sink, and without other voids and dislocations, the swelling rate is large near the permanent sink, and reaches a constant lower

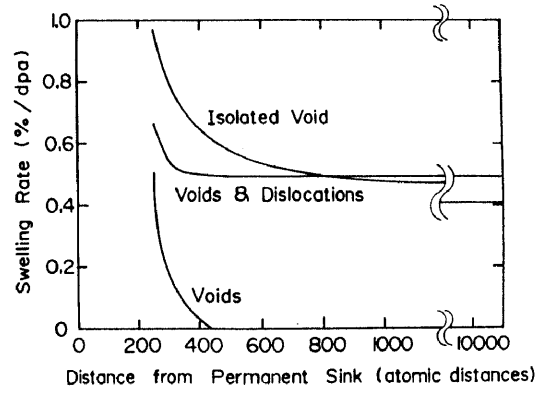

Fig. 8. The variation of void swelling rate at 10 % swelling in three cases as a function of the distance from the neutral permanent sink.

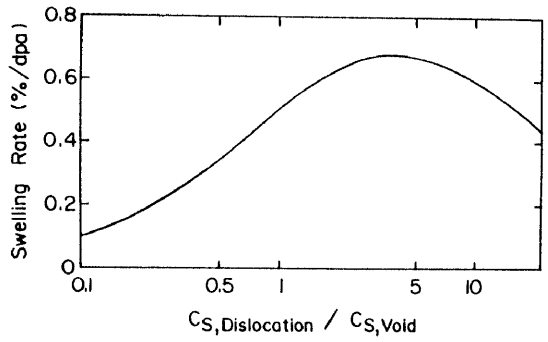

Fig. 9. The variation of the void swelling rate at 10 % swelling as the function of the ratio of dislocation sink strength to void sink strength.

value with increasing distance from the sink. In the case of coexistence of voids and dislocations with the same sink strength, void growth saturates at a certain level. The level is determined by the ratio of the sink strengths between voids and dislocations.

Synergistic effects with dislocation bias are discussed. For the growth of voids by CLIB, the existence of sinks other than voids is required, such as dislocations, though dislocation bias is not required. In the simplest case of a high density of voids without any other sinks, the growth of the shrinkage of other voids by the absorption of extra interstitials sent from the former. Fig. 9 shows the variation of void swelling rate as a function of the ratio of the dislocation sink strength to void sink strength. With increasing dislocation sink strength, the void swelling rate first increases, and then decreases. The decrease is caused by excess absorption of both types of point defects by dislocations.

4. Influence of Primary Recoil Energy Spectrum on Microstructural Evolution[9)]

In order to decompose the effect on microstructure evolution from a wide recoil energy spectrum of neutron irradiation, self-ion irradiation with variable energy is performed. Even from the same energy of self-ions, there was found a wide variation in the formation of vacancy clusters. The number of groups of vacancy clusters, forming closely spaced groups in Ag and A, monotonically decreases to the larger groups as shown in Fig. 10, without showing a peak. When the total number of vacancy cluster groups (including isolated ones) is compared with the number of incident ions, an appreciable percentage is found not to have formed visible defects, as shown by zero-size in the figure. With the increase of ion energy, the percentage of these invisible cascades decreases and the grouped defect clusters extends to larger numbers.

Binary collision simulation of subcascade formation is made in parallel with experiments. Computer simulation by binary collision approximation also showed a wide distribution of the number of subcascades produced by PKAs with same energy as shown in Fig. 11. Difference of the distributions of observable vacancy clusters in self-ion irradiation from these computed ones is is in the monotonic decrease towards greater groups of vacancy clusters, whereas the computed results have a peak which shifts towards a larger number of subcascades for larger PKA energy. The major reason for this difference is thought to be in those subcascades which have not shown up as visible clusters.

Microstructure formed by 14 MeV neutron irradiation

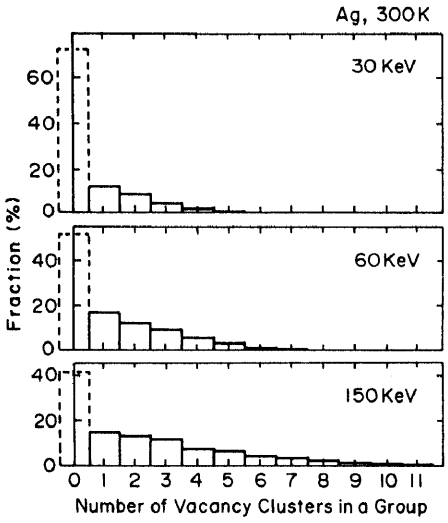

Fig. 10. Closely spaced vacancy groups formed in self-ion irradiated Ag for four ion energies. The values at zero size were obtained from the total number of incident ions as those not contributing to the formation of visible clusters.

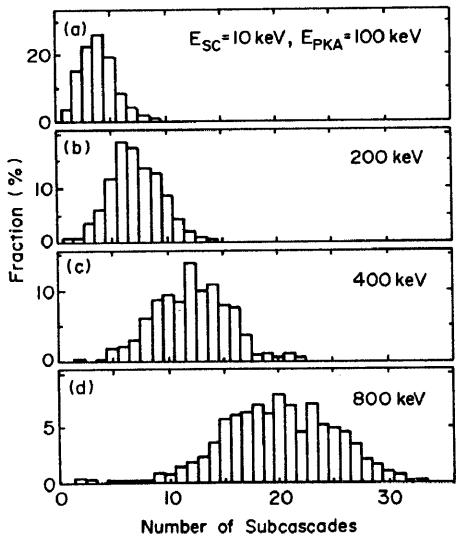

Fig. 11. Distribution of the number of subcascades produced in Cu by binary collision approximation simulation. Subcascade threshold energy adopted was 10 KeV.

is reconstructed both from self-ion irradiation data and from collision simulation data. The distribution of vacancy cluster groups corresponding to the primary recoil energy spectrum in 14 MeV neutron irradiation has been reconstructed, and shown in Fig. 12. The result is compared with the experimentally observed distribution in the same figure, and the agreement between the two is found to be satisfactory. The same procedure of reconstruction of group size distribution has been carried out for the computer simulated subcascades, again quoted from a paper. Fig. 13 is the comparison with experimental observation in copper. The computed result with the assumption of 10 keV for subcascade energy fits well to the observed one. This subcascade energy of 10 keV for copper is the value which was obtained from the recoil energy spectrum analysis with the simplest assumption of no distribution from same PKA. The simplest analysis cannot be said to be meaningless.

The concept of subcascade formation is reconsidered from the viewpoint of microstructural evolution. Examination of the extremely small success probability of cascade collision induced interstitial cluster nuclei to grow into dislocation loops leads to a proposal of the important role of stochastic fluctuation of point defect reaction. Various

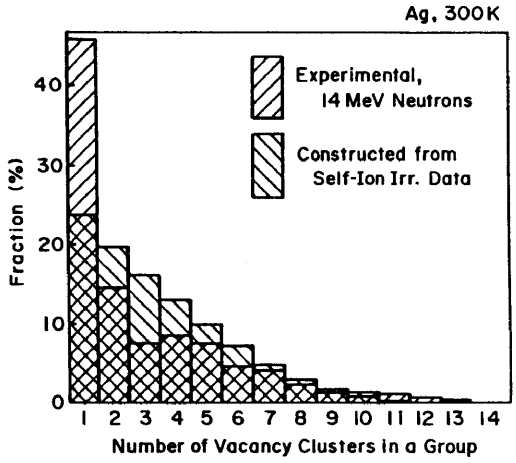

Fig. 12. Comparison of subcascade distribution expected in 14 MeV neutron irradiation constructed from self-ion irradiation data with experimental observation of 14 MeV neutron irradiation.

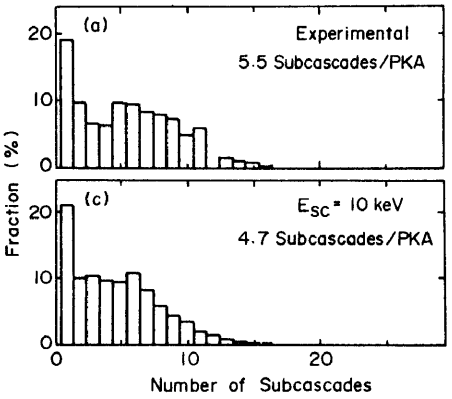

Fig. 13. Distribution of the number of subcascades in 14 MeV neutron irradiated copper. (a) Experimental analysis, and (b) model calculation with the subcascade threshold energy of 10 keV.

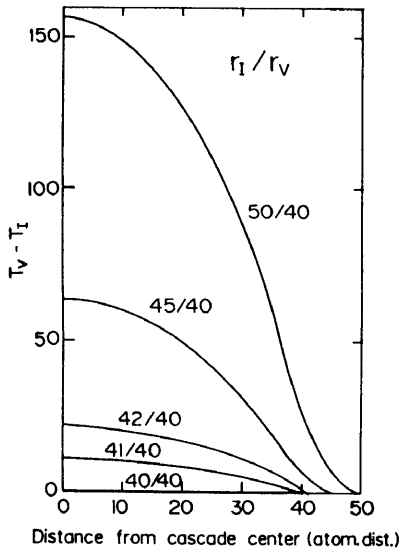

Fig. 14. Estimation of T_V-T_I for various values of r_I/r_V with constant r_V as a function of the distance from the center of cascade.

sources which cause the unbalanced reaction of vacancies and interstitials are examined: interstitial predominance by vacancy cluster formation, vacancy predominance by interstitial cluster formation, and a particular emphasis on the cascade localization induced bias effect.

5. The Variation of the Cascade Localization Induced Bias Effect with Material Parameters and Irradiation Conditions[17]

The distribution of vacancies and interstitials produced by collision cascades is expected to be highly condensed with vacancies surrounded by interstitials. The effect, which comes from the imbalance of reactions between vacancies and interstitials originating from the difference of the initial distribution of point defects (cascade localization induced bias, CLIB), is examined with a method based on the solution of the diffusion equation of cascade dissipation with a variety of initial condition. The strength of CLIB is defined as the difference of jumps between interstitials and vacancies before their annihilation. The variation of the strength with material parameters and irradiation condition is estimated.

If we define the integrated migration efficiency as $T_T = M_V C_V dt$ and $T_I = M_I dt$, the shrinkage or growth of a defect cluster is determined by $Z_{VC}T_V$-$Z_{IC}T_I$. In the following treatment, the strength of CLIB for the defect structure evolution under various irradiation conditions is estimated by T_V-T_I. The difference of the integrated migration efficiency T_V-T_I is shown in Figs. 14 and 15 ass functions of position from the center of a cascade and the initial distributions of interstitials and vacancies.

A parameter S is defined as

$$S = \int \frac{T_V - T_I}{V C_{10}} dv$$

The change of S as a function of the difference of two distributions is shown in Table 1 keeping the r_V constant. The value S increases remarkably with increasing the difference. Table 2 shows the case of the constant difference of two point defect distributions. With increasing vacancy

Table 2. Estimation of S and void growth rate at 10 % swelling for various values of r_I/r_V with constant r_I-r_V.

r_I/r_V	30/10	40/20	60/40	100/80	200/180	500/480
S	3.1	4.8	8.0	14.3	30.2	78.0
Growth rate [%/dpa]	0.17	0.31	0.54	0.90	1.62	3.38

Table 1. Estimation of S and void growth rate at 10 % swelling for various values of r_I/r_V with constant r_V.

r_I/r_V	40/40	60/40	80/40	100/40	200/40	500/40
S	0.0	8.0	19.1	33.4	152.8	988.3
Growth rate [%/dpa]	0.0	0.542	0.91	1.18	1.93	2.63

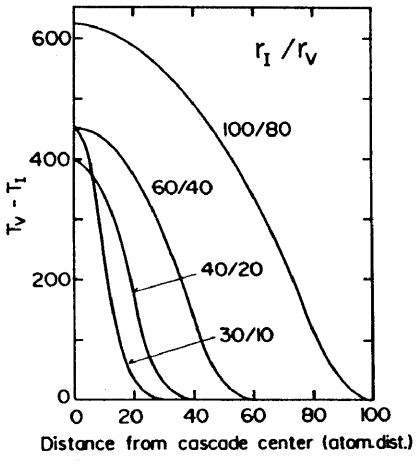

Fig. 15. Estimation of T_V-T_I for various values of r_I/r_V with constant r_I-r_V, as a function of the distance from the center of cascade.

region, the value S also increases remarkably. The void growth rate at the same cascade conditions are shown in the lower column of each table. Here in these tables, we can observe that the strength is higher in larger cascades than in smaller ones if the difference of the distributions is the same. It is also higher in compact cascades such as in Au and Ag than in dilute cascades such as Al and Fe because of the difference of the initial distributions. In subcascade structures, as in Cu and Ni, CLIB occurs in each subcascade and the effect per damage energy is not changed by PKA energy.

6. Fluctuation Effect of Point Defect Reaction on Nucleation of Interstitial Clusters during Neutron Irradiation[18]

Effects of stochastic fluctuation of point defect reaction on the destination of small interstitial clusters were discussed.

Nuclei of interstitial clusters are known to be formed directly from cascade collisions during neutron irradiation. However, the number of experimentally observed interstitial clusters is always much less than the number of cascade collisions in all the materials observed. Number density of interstitial loops in thin foil nickel irradiated by fission neutrons in the Japan Materials Testing Reactor (JMTR) is shown in Table 3. In this irradiation, neutron collision

Table 3. Number density of interstitial loops and its fraction to the number of PKA in fission neutron irradiated thin foil nickel.

	473 K	573 K
(a) Number density [loops/m^3]	3×10^{22}	9×10^{21}
(b) Neutron fluence [n/m^2] ($E > 1$ MeV)	2.5×10^{23}	3.7×10^{23}
(c) PKA (> 10 keV) [PKA/m^3]	1.2×10^{25}	1.6×10^{25}
(d) (a)/(c)	3×10^{-3}	6×10^{-4}

Table 4. Fraction of the number density of interstitial loops to the number of PKA in 14 MeV neutron irradiated nickel at 473 K.

	Neutron dose [$\times 10^{22}$ n/m^2]		
	0.9	1.6	4.3
Thin foil	4×10^{-2}	5.6×10^{-2}	4.6×10^{-2}
Bulk	4×10^{-4}	4.1×10^{-4}	1.5×10^{-4}

cross-section that gives more than 10 keV to a primary knock-on atom (PKA) is 0.9 barns. Fraction of the number of loops to the number of cascade collisions (>10 keV) is less than 1 % as shown in the table. The fraction becomes even smaller in the case of bulk irradiated materials. Fraction of the number of interstitial clusters in thin foil and large interstitial loops in bulk to the number of cascade collisions (>10 keV) at each neutron fluence is listed in Table 4. Thus the success fraction of interstitial cluster nuclei for growth was less than 1/10 in thin foil irradiated samples and less than 1/1000 in bulk irradiated samples, even in the atmosphere of excess free interstitials.

The situation mentioned above cannot be explained by rate theory, and stochastic fluctuation of the absorption of free vacancies and interstitials is expected to be playing the major role. Fig. 16 shows the variation of the size of vacancy clustered defects in the shape of stacking fault tetrahedra (SFT) in copper during electron irradiation with a high voltage electron microscope. This fluctuation of the size is considered to occur by the stochastic fluctuation of the absorption of vacancies and interstitials. The origin of the fluctuation is expected both in the randomness of the birthplace of point defects by electron collision and in the random diffusion path of the defects. The repetition of the

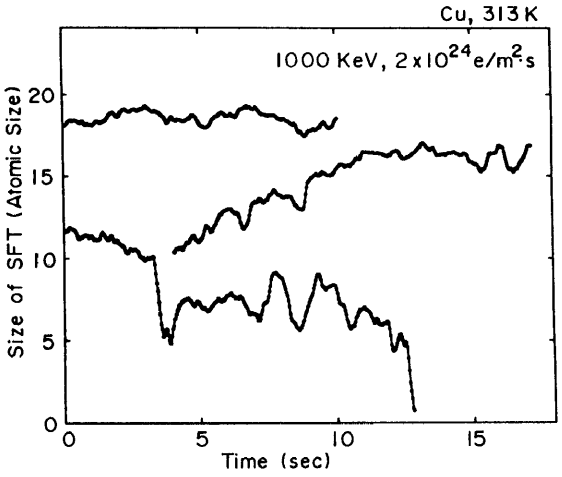

Fig. 16. Variation of the size of stacking fault t tetrahedra in copper during electron irradiation with a high voltage electron microscope.

shrinkage and growth occasionally make a small cluster shrink to zero size. The success probability of interstitial clusters for growth is expected to be suppressed to an extremely low level.

7. Binary Collision Calculation of Subcascade Structure and its Correspondence to Observed Subcascade Defects in 14 MeV Neutron Irradiated Copper[19]

A model calculation of subcascade structure in copper, based on the binary collision approximation using MARLOWE code, is made. The primary recoil energy spectrum by 14 MeV neutron irradiation and the threshold

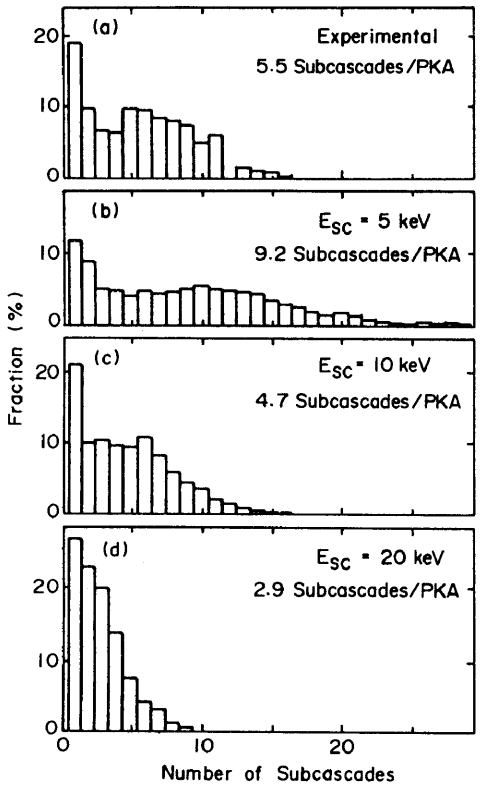

Fig. 17 Distribution of the number of subcascades in 14 MeV neutron irradiated copper: (a) experimental analysis, and (b)-(d) model calculation by MARLOWE with the subcascade threshold energy Esc of 5, 10 and 20 keV.

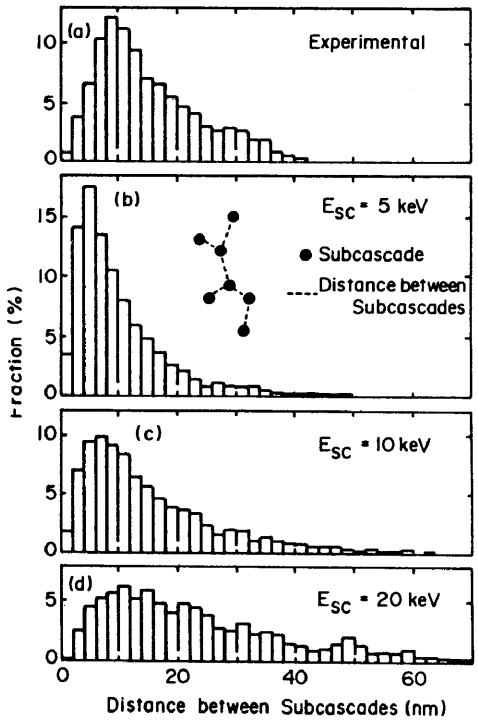

Fig. 18. Distribution of the distance between subcascades in 14 MeV neutron irradiated copper: (a) experimental analysis, and (b)-(d) model calculation by MARLOWE with the subcascade threshold energy E_{SC} of 5, 10 and 20 keV

type subcascade energy of 10 keV are employed. The calculated results of the number of subcascades and the distance between subcascades show good agreement to reported experimental analysis.

Distribution of the number of subcascades produced from PKA spectrum of 14 MeV neutrons is shown in Fig. 17. Fig. 17 (a) is the result of experimental analysis. Figs. 17 (b), (c) and (d) are the calculated results, assuming the subcascade threshold energy, E_{SC}, as 5, 10 and 20 keV, respectively. The average number of subcascades per PKA is also shown in the figure. The calculation with E_{SC}=10 keV for the subcascade energy gives a fairly good correspondence to the experiment.

Distribution of the distance between subcascades are shown in Fig. 18. Subcascades are shown in Fig. 18. Subcascades with closer mutual distance are chained to each other, until all the subcascades are connected through these chains, which is schematically shown in Fig. 18 (b) by broken lines. When a cascade consist of N subcascades, number of chains is (N-1). The length of each chain is measured as distance between subcascades. A tendency of the larger distance at larger subcascade threshold energy is observed.

Distribution of the calculated cascade zone size extends towards larger size much more than that experimentally obtained for thin foil irradiation. Fig. 19 is the distribution of the cascade zone size. The size is defined as the diameter of the smallest sphere which contains all the subcascades in a cascade, and is comparable to the range of the PKA. Fig. 19 (a) is the result of the experimental analysis. Fig. 19 (b) is the result of the model calculation with E_{SC}=10 keV. The correspondence between the experiment and the calculation is not as good as in the case of the number of subcascades and the distance between subcascades. This difference is understood as the under estimation in

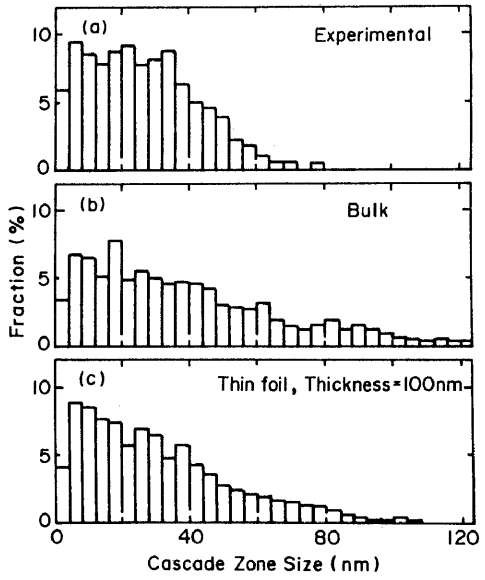

Fig. 19. Distribution of the cascade zone size in 14 MeV neutron irradiated copper: (a) experimental analysis, and (b) model calculation by MARLOWE with the subcascade threshold energy E_{SC} of 10 keV, and (c) model calculation with the specimen foil thickness of 100 nm, E_{SC}=10 keV.

experimental measurement owing to the limitation by the thickness of the microscopically observable specimen foil (<100 nm).

Distribution of subcascade structure produced by monochromatic primary recoil energy is examined by the same calculation model. Distribution of the number of subcascades produced by monochromatic primary recoil energies of 100, 200, 400 and 800 keV are shown in Fig. 20. The subcascade threshold energy E_{SC} is fixed to be 10 keV in all of the present calculations. The average number and the half width of the distribution is plotted against the damage energy in Fig. 21. The average number of subcascades is nearly proportional to the damage energy. it is clearly observed that constant primary recoil energy produces a wide range of the number of subcascades. The

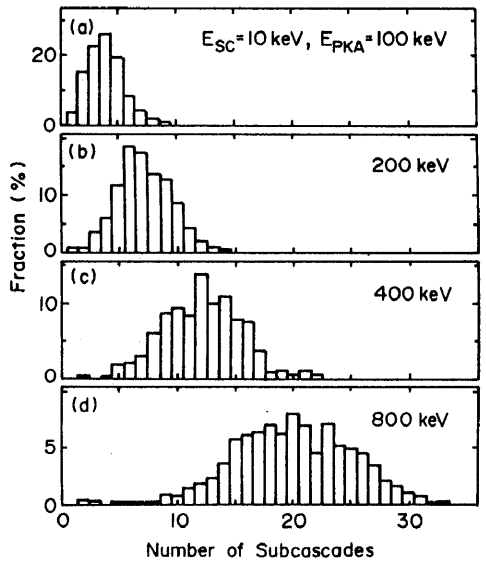

Fig. 20. Distribution of the number of subcascades under the primary recoil energy E_{PKA} of (a) 100 keV, (b) 200 keV, (c) 400 keV and (d) 800 keV calculated by MARLOWE with the subcascade threshold energy Esc of 10 keV.

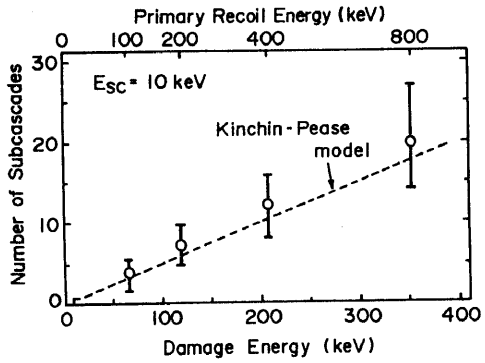

Fig. 21. Relation between the calculated number of subcascades by MARLOWE code and the damage energy. The number of subcascade according to the Kinchin-Pease model is also shown by the broken line.

broader distribution at the higher primary recoil energy is also observed. The number of subcascades derived from the Kinchin-Pease model with the threshold energy of 10 keV, which was applied in the experimental analysis, is also shown in the figure. The Kinchin-Pease model gives nearly the same result to the average number of subcascades as the MARLOWE.

8. Detection of the Role of Free Point Defects from the Variation of Defect Structures near Permanent Sinks in Neutron Irradiated Metals[20]

The role of freely migrating point defects during neutron irradiation in the defect structure development with the presence of permanent sinks is studied using rate equations. Three specific cases are examined as a function of the distance from the surface: (1) only interstitial cluster existing system, (2) interstitial cluster and vacancy cluster coexisting system, and (3) only vacancy cluster existing system.

Easy formation of interstitial clusters in thin specimen, and near the surface and the grain boundary of thick specimen. The variation of migration efficiencies M_IC_I and M_VC_V at the center of the specimens are shown in Fig. 22 for thin and thick specimens, i. e., 200 and 1.1×10^5 atomic distances. In the case of a thick specimen, with increasing irradiation time, first C_I reaches its quasi-steady state and

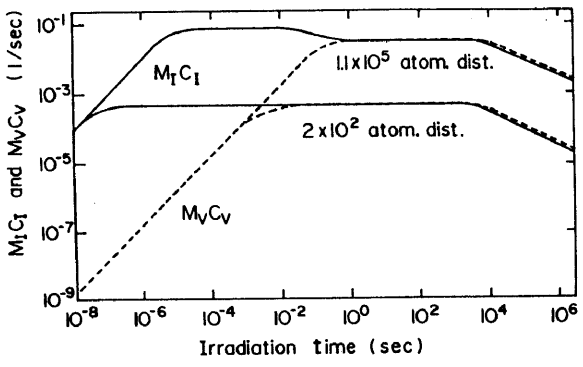

Fig. 22. The variations of migration efficiencies M_IC_I and M_VC_V at the center of thin specimen of 2×10^2 atomic distances and thick specimen of 1.1×10^5 atomic distances in only interstitial loop existing system.

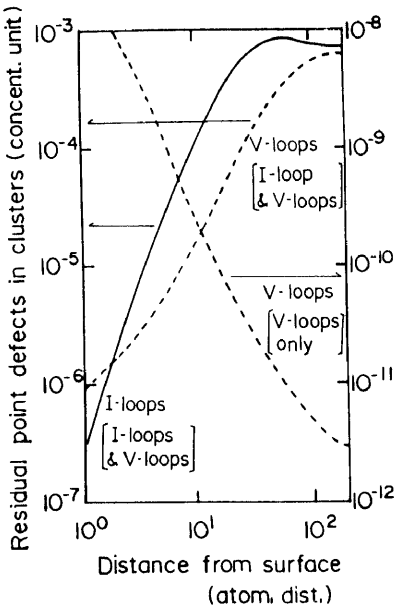

Fig. 23. The residual point defects in clusters after neutron irradiation of $2x10^6$ s as a function of the distance from the surface in only vacancy loop existing system and vacancy loop and interstitial loop coexisting system.

keeps its level until $t=10^{-2}$s. Because of lower mobility of vacancies, it takes 10^{-1} s to reach its quasi-steady state, and C_I decreases at the same time owing to the mutual annihilation. The quasi-steady state is destroyed by increasing point defect clusters. The growth rate is high when C_I reaches its maximum value, and keeps the rate for a while until vacancies begin to play a role.

Easy formation of interstitial clusters in thin specimen, and near surface and the grain boundary of thick specimen just the same as those in case (1) but the growth of both types of clusters in the deeper region of thick specimen.

Easy formation of vacancy clusters near the surface of the specimen. The defect structure evolution in only vacancy loop existing system is calculated as shown in Fig. 23 (V-loops [V-loops only]). The total number of residual point defects, vacancies, is low and decreases with increasing distance from the surface. As for comparison, the total numbers of residual defects in both interstitial loop and vacancy loop existing system are also shown in the figure. They increase with increasing the distance from the surface. When interstitials can not form clusters, free interstitials play a role to annihilate vacancy clusters, especially in deeper region because of less escape of them to the surfaces.

9. Low Dose Fission Nneutron Irradiation on P- and Ti- Modified Austenitic Alloys with Improved Temperature Control[21]

The initial process of microstructure evolution in Fe-16Cr-17Ni and its P- and Ti-modified variants was studied during irradiation in JMTR to 1.1x1024 n/m^2 (>1.0 MeV) under improved and conventional temperature control conditions. Interstitial loop density showed strong temperature dependence. Weak beam dark-field images in Fig. 24 show typical microstructures formed at 473, 573, 623 and 673 K. Dislocation loops, stacking fault tetrahedra and voids were observed depending on the irradiation temperature. Nominal activation energy for the loop nucleation process in the ternary alloy was about 0.5 eV.

With addition of 0.024%P, the interstitial loop density increased very much, but void formation was suppressed considerably. In 0.1%P-alloy, Fe_2P was precipitated at 673 K instead of interstitial loops. In conventional temperature control irradiation, loop density was two to three times higher than that of improved control irradiation. This suggests the need for improvement of temperature control of fission reactor irradiation for understanding essential processes of damage evolution at the set temperature.

10. The Role of Free Point Defects in Defect Structure Evolution during Cascade Damage[22]

High energy particle irradiation is performed for Au, Cu and Ni with fission neutrons and fusion neutrons at temperatures above 473K. The role of free point defects in defect structure evolution during cascade damage is studied by electron microscopy, by observing the variation of defect structure evolution with sink geometry and the thermal

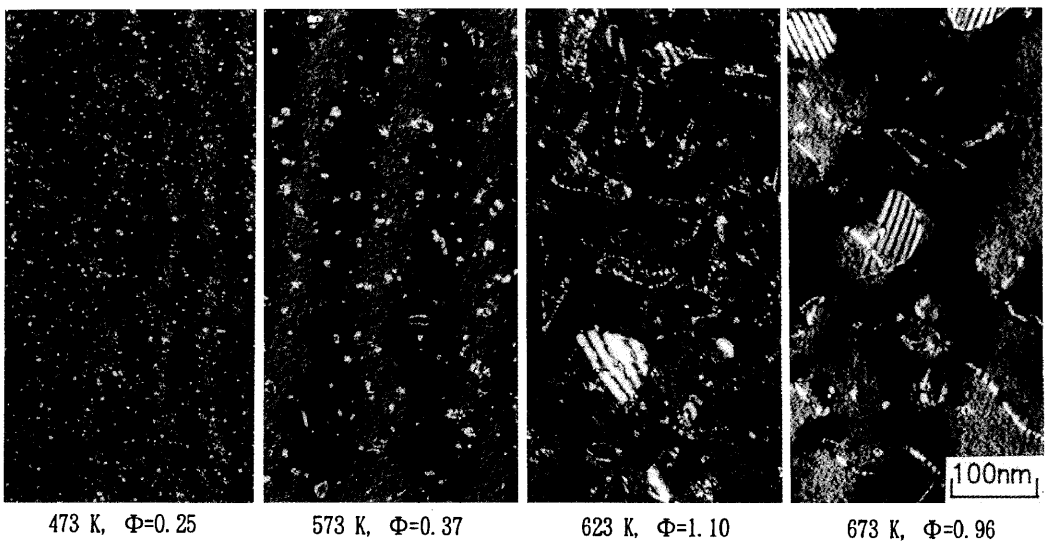

Fig. 24. Dark field weak beam images of microstructures formed by neutron irradiation with improved temperature control at various temperatures.

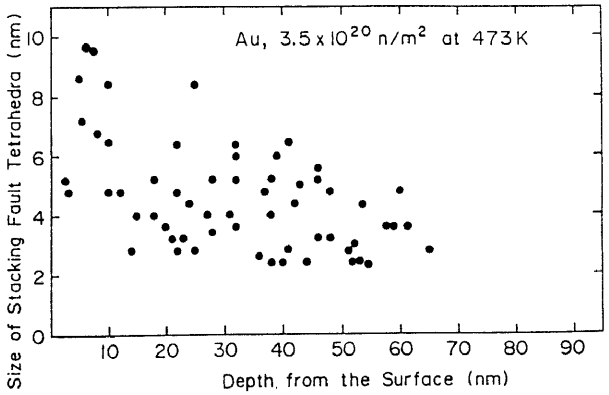

Fig. 25. The size and their position of stacking fault tetrahedra after neutron irradiation of 3.5×10^{20} n/m^2.

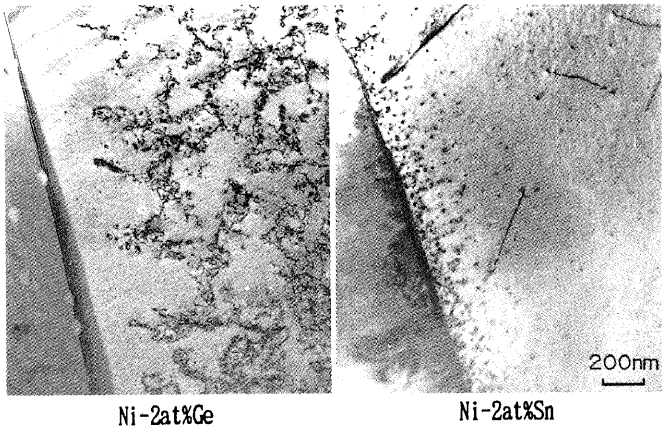

Fig. 26. Defect structures near grain boundaries in bulk irradiated Ni-2at%Sn and Ni-2at%Ge at 573 K by fission neutrons with JMTR to a dose of 3.7×10^{23} n/m^2 (>1.0 MeV).

stability of point defect clusters. Results obtained are as follows.

When only one type of point defect clusters is thermally stable, the clusters are formed preferentially near surfaces and grain boundaries. In the case of Au at above 473 K only vacancy type point defect clusters, stacking fault tetrahedra, were formed directly in the cascade area. They were observed only near surfaces of the specimen as in the measured result of size and position from the surface in Fig. 25. The size of stacking fault tetrahedra was larger near the surface and no stacking fault tetrahedra were observed deeper area than 65 nm from the surface. By the cascade damage, exactly the same amount of interstitials and vacancies are originally produced. Near the surface, interstitials can promptly escape to the surface, and stacking fault tetrahedra survive with their original size. On the other hand at the inner area, more number of interstitials than vacancies are absorbed by stacking fault tetrahedra, consequently stacking fault tetrahedra shrink at the deeper area. At lower temperatures, for example below 363 k for Au, both interstitial loops and stacking fault tetrahedra were formed as stable point defect clusters in cascade. in this case an annihilation of stacking fault tetrahedra at the inner area was not so remarkable, because of the consumption of some interstitials in their cluster formation.

Fig. 26 shows defect structure evolution near grain boundaries of dilute nickel alloys after fission neutron irradiation at 573 K using JMTR. Many interstitial type dislocation loops were observed in a restricted area near grain boundaries in Ni-2at%Sn. At the area very close to the grain boundary, the nuclei of interstitial loops formed in cascades stay small because of the low concentration of interstitials. With increasing the distance from the boundary, interstitial loops can grow by the preferential absorption of interstitials. At the area far from the grain boundary, the grain boundary does not act as a sink any more, and interstitial loops formed at cascades are only sink for point defects. Loops absorb the same amount of interstitials and vacancies, and they cannot grow large.

In Ni-2at%Ge, high densities of voids and dislocation networks were observed at an area far from grain boundaries as shown in Fig. 26 (b). These dislocation networks were developed by an extensive growth of interstitial loops. In this material, small interstitial loops and voids are thermally stable, and interstitial loops grow large by absorption of more interstitials than vacancies by their bias, and excess vacancies accumulated in voids.

Preferential formation of interstitial loops near edge dislocations occurs when the loop formation in the dislocation free matrix is almost difficult. Preferential progress of interstitial loop formation was observed at one side of edge dislocations (dilatatinal side) as shown in Fig. 27. This phenomena is one of the most clear evidences for the nucleation of interstitial clusters at cascades in neutron irradiation, because the phenomena is suppressed near sinks

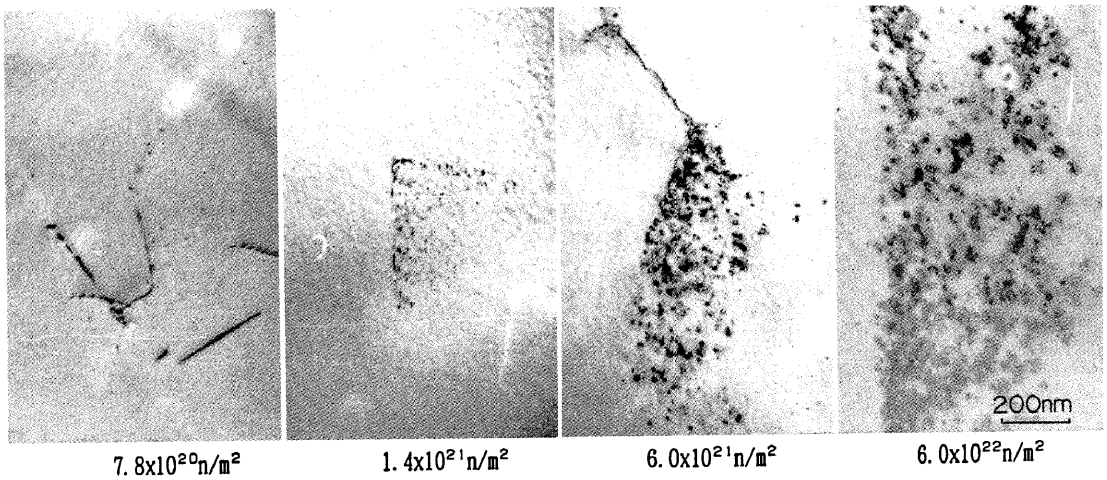

Fig. 27. Preferential formation of interstitial loops near edge dislocations in D-T fusion neutron irradiated Ni-2at%Cu as a bulk at 563 k with RTNS-II to a dose of 3×10^{22} n/m^2.

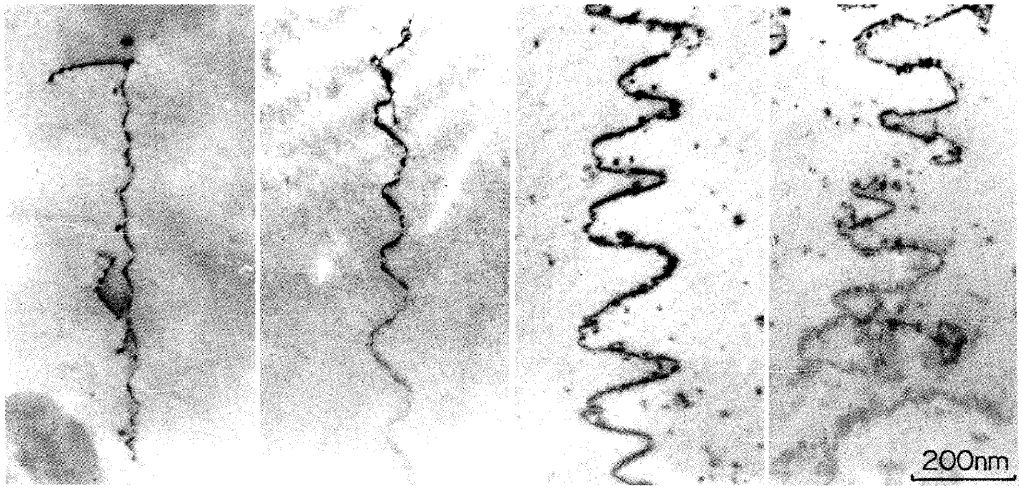

Fig. 28. Growth of helical dislocations in D-T fusion neutron irradiated Ni as a bulk at 563 K to a dose of $6.2 \times 10^{22}/m^2$.

in the case of homogeneous point defect introduction as in the case of electron irradiation.

The development of helical dislocations suggests a possibility to measure numerically the reaction of free point defects during irradiation. Fig. 28 shows fusion neutron irradiated Ni at 563 K. With increasing irradiation dose the screw dislocations become helical. The growth of helix is the difference of point defect absorption between interstitials and vacancies, and has a possibility to be used for the measurement of the amount of free point defects during irradiation, eliminating the ambiguity in the measurement by dislocation loops whose nucleation during irradiation cannot be well defined.

11. Origin of Unbalanced Reaction of Vacancies and Interstitial during Irradiation with Cascades and Influence on Microstructural Evolution[23]

Based upon the underlying premise that all the microstructure evolution during irradiation results from the asymmetrical reaction between vacancies and interstitial, the origin of the asymmetry is sought and categorized, and the mechanism of defect structure evolution for each source of asymmetry is investigated. The role of neutral sinks and the influence of dislocations are examined for the cases of irradiation with and without cascade damage. Vacancy cluster formation directly from cascades is found to favor the generation of freely migrating interstitial. Stochastic fluctuations of the point defect reactions under the balanced condition of vacancy and interstitial is experimentally defected, and the important role of the fluctuations is found in the determination of the fate of small interstitial cluster embryos produced by cascade damage. The influence of the unbalanced point defect reaction starting from difference in spatial distribution between vacancies and interstitials formed by cascade collisions is discussed as one of the important origins of vacancy dominant reactions.

12. Influence of Details of Reactor History on Microstructural Development during Neutron Irradiation[4]

Microstructually-oriented irradiation experiments are shown in this paper to be strongly dependent on details of reactor history that frequently are not brought to the experimenter's attention. In some cases, these details can dominate the experiment so as to produce very misleading results. To aid in the design and interpretation of microstructurally-oriented experiments, a number of studies are reviewed to highlight history effects and then guidelines are presented to minimize the impact of reactor history in new experiments.

13. Exposure Time and Recoil Energy Dependence of Defect Accumulation[6]

Experimental information from irradiations with a wide variety of energetic particles, electrons, ions and fission and fusion neutrons, is combined and analyzed to elucidate the mechanism of microstructure evolution during irradiation, with particular interest placed on the case of cascade damage. The rapidly progressing understanding of the time dependence of microstructural evolution in metals within the low irradiation dose regime is reviewed, and a proposal will be made for an improved fission reactor irradiation at the end.

13.1. Time evolution of defect structures during homogeneous entroduction of vacancies and interstitials

Partly intending to serve as a reference to the discussion of the major part of this paper on irradiations with heavy particles, a brief survey was made on the point defect reaction kinetics during electron irradiation. Reaction kinetics of point defects during homogeneous introduction of interstitials and vacancies was explained focusing the time evolution of the reaction processes. Nucleation of interstitial clusters was utilized to obtain the migration property of interstitials, and the growth of interstitial clusters was utilized to obtain the motion properties of vacancies.

Stochastic fluctuation of point defect reaction was detected during electron irradiation. Fig. 29 is an example of series micrographs of repetition of the growth of stacking fault tetrahedra by the absorption of vacancies and shrinkage by the absorption of interstitial atoms. All the

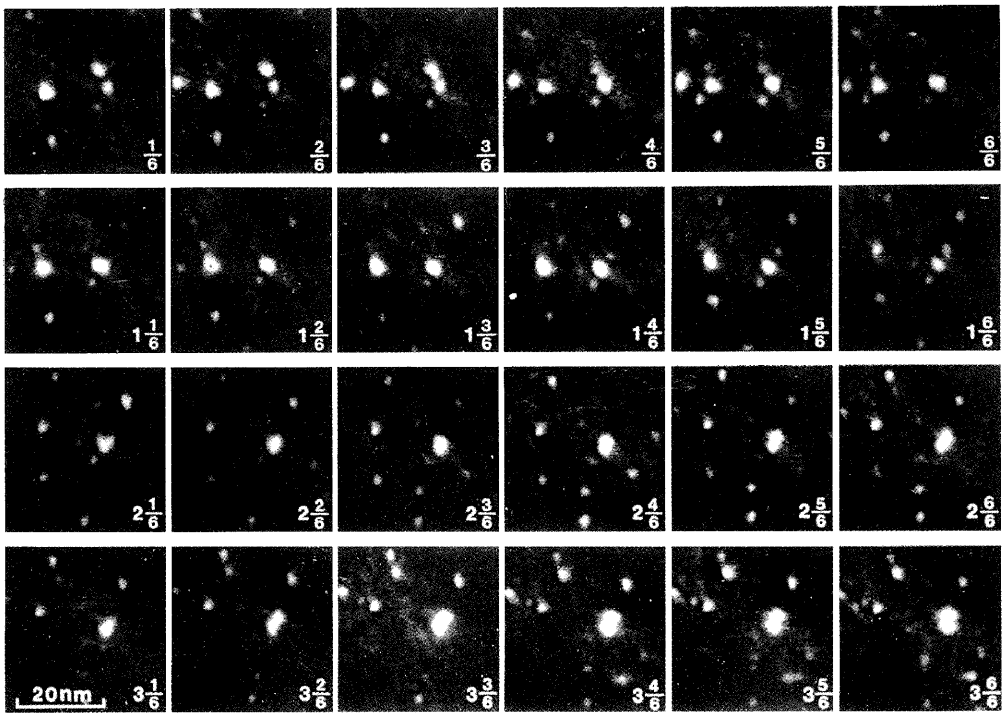

Fig. 29. Repeated growth and shrinkage of vacancy clusters in copper under electron irradiation. 1000 keV, $2x10^{23}e/m^2s$ at 300 K. Indicated is the irradiation time in seconds (not started from zero second).

clusters eventually disappear reaching to size zero. Point defects generated by the collision of electrons are not homogeneously distributed but are located at random, and the diffusion path of each point defect after the generation is again at random. Consequently, the flux of vacancies and interstitials to a given lattice site are not equal to each other but instead fluctuate when examined over a short period of time.

Positional instability of small interstitial clusters was detected during electron irradiation. in many fcc metals and also in some bcc metals, small interstitial clusters in the form of dislocation loops make an intermittent quick motion about a distance comparable to the mutual separation between neighboring loops. it is not easy to show this phenomena with frame pictures, but Fig. 30 shows at lease that many loops have changed their position during irradiation. Recent observation and analysis have shown that the motion of the loops in fcc metals is along [110] direction and is not on the plane of the loop.

13.2. Categorized typical cases of time dependence of vacancy cluster accumulation during irradiation damage with cascade.

A kinetic analysis is made for each of the categorized cases of time evolution of defect structures during irradiation with cascade damage. Fig. 31 shows the progressive variation of the time dependence of accumulation of vacancy clustered defects, in which four typical stages of the irradiation time dependence are schematically illustrated. Stage I at the lowest dose range is proportional to the square

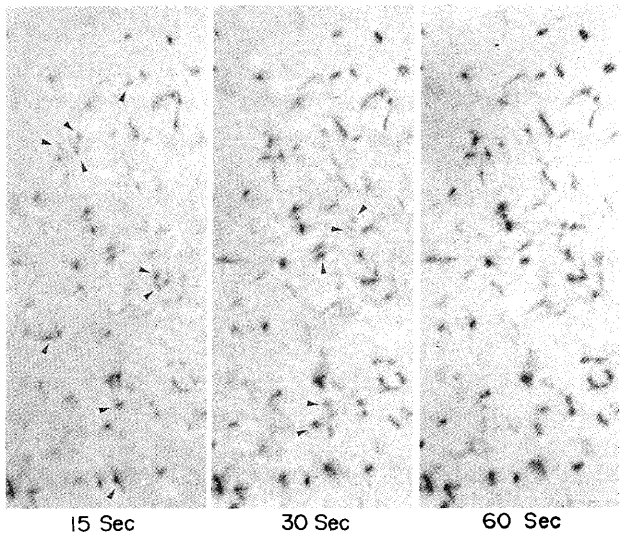

Fig. 30. Intermittent motion of small interstitial clusters observed during electron irradiation. Interstitial clusters pointed by arrowheads are observed to have moved in the next micrograph. Ni, 1000 keV, $5x10^{23}e/m2s$ at 300 K.

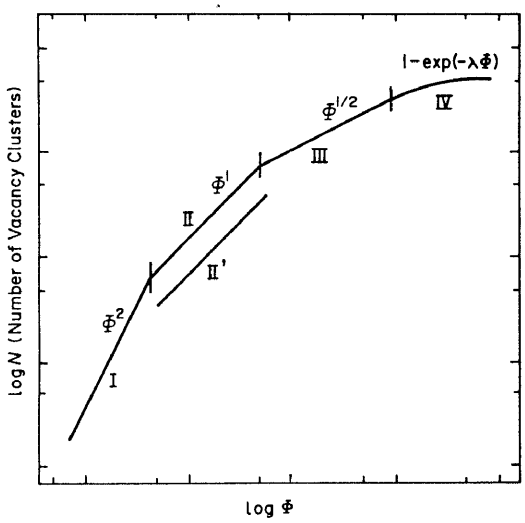

Fig. 31. Progressive variation of the accumulation of vacancy clusters produced by cascades. All the stages from I to V do not necessarily appear depending on irradiation conditions.

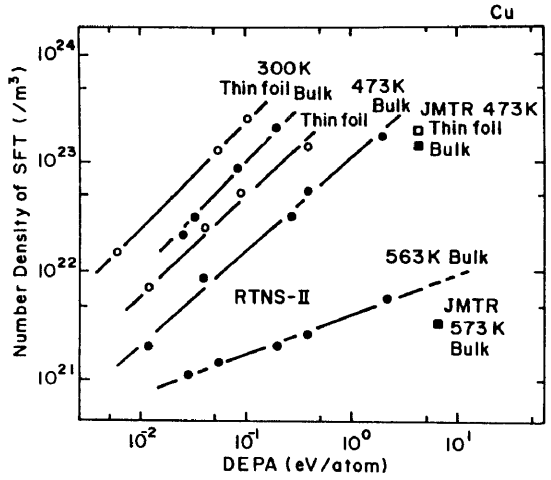

Fig. 32. Variation of the mode of accumulation of vacancy clustered defects in 14 MeV neutron irradiated copper with the specimen geometry (thin foil or bulk) and irradiation temperature. Some fission neutron irradiation (JMTR) data are also shown.

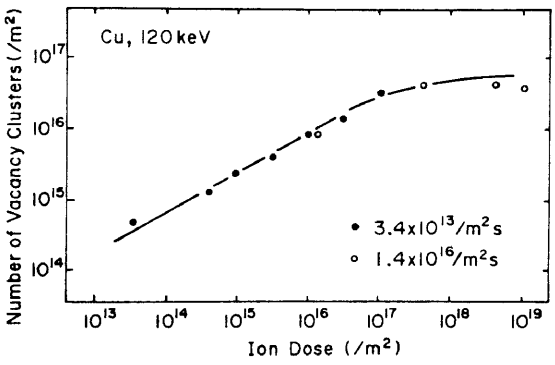

Fig. 33. Accumulation of vacancy clusters at room temperature in self-ion irradiated copper. Solid line is from the random overlap analysis.

of the irradiation dose, during which the formation of vacancy cluster s from cascade needs a help to impact from other cascades. Lower dose range in Fig. 4 shows this stage. The second, Stage II, is simply proportional to the irradiation dose, during which all the vacancy clusters formed directly from cascades are preserved. Stage II' is also proportional to the irradiation dose, but the accumulation rate is smaller than in the case of Stage II, owing to the continuous annihilation of existing vacancy clusters by freely migrating interstitials which have not been absorbed to interstitial clusters. Stage III is proportional to the square root of the irradiation dose and is typical of irradiation effects in which one species of point defects do not form their clusters at all and they continuously annihilate the clusters of other species of
point defects, vacancy clusters in the present case. Fig. 32 contains examples of the Stage, II, II' and III. The final stage, Stage IV, the number of vacancy clusters exponentially saturates to a certain level by the geometrical overlap of cascades, simply annihilating vacancy clusters by interstitials released from cascades produced at its vicinity. Fig. 33 shows an example of this Stage III.

13.3. Evolution of interstitial type defect structures during irradiation with cascade damage

Even when one accepts the nucleation of interstitials clusters in displacement cascades, except for the case of very low temperate irradiation, the number of interstitial clusters which succeed to grow into dislocation loops is many orders of magnitude smaller than the number of large cascades as shown in an example of Fig. 34. This extremely small success probability of small interstitial cluster to grow to observable dislocation loops is difficult to be accounted by reaction kinetics type of analysis, and two separate effects which might have essential roles to prevent the clusters to grow large will be explained here: the one is the fluctuation of point defect reaction and the other is the positional instability of small interstitial clusters, both explained in 13.1.

When a balanced condition is established by the production of the same number of freely migrating interstitials and vacancies, small interstitial clusters produced at cascades, named here as interstitial cluster embryo, embryo should be able to grow by their attractive interaction to interstitials. Thus, the very small experimentally observed success ration for growth can never be expected from the normal kinetics type analysis of point defect reaction. Here, the fluctuation of point defect reaction is introduced to play a role to determine the fate of small point defect clusters.

Simulations with computer generated random numbers were made to obtain the percentage of embryos to grow after many reactions. The survival ratio naturally decreased for smaller initial size, 6.9, 5.3, 3.5 and 1.4 % for the initial size in the number of interstitial atom unit of 20, 15, 10 and 5, respectively.

When one accepts to apply the positional instability of small interstitial clusters, observed during electron irradiation explained in 13.1, to the case of cascade damage, the definitive analysis of the survival ration of interstitial clusters formed from cascades may become very difficult.

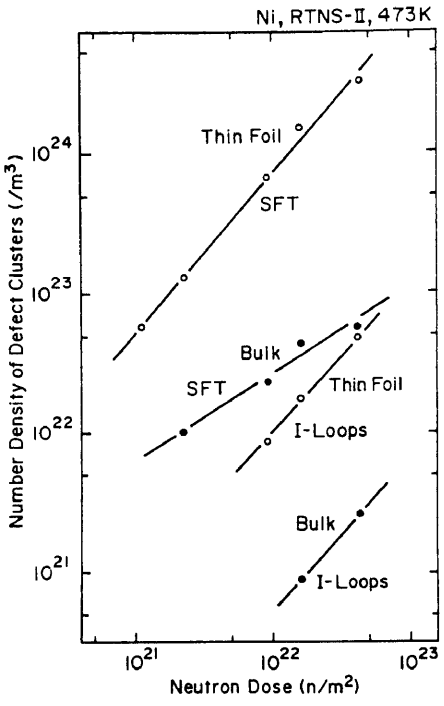

Fig. 34. Variation of the mode of accumulation of point defect clusters in 14 MeV neutron irradiated nickel with the specimen geometry (thin foil or bulk) at 473 K.

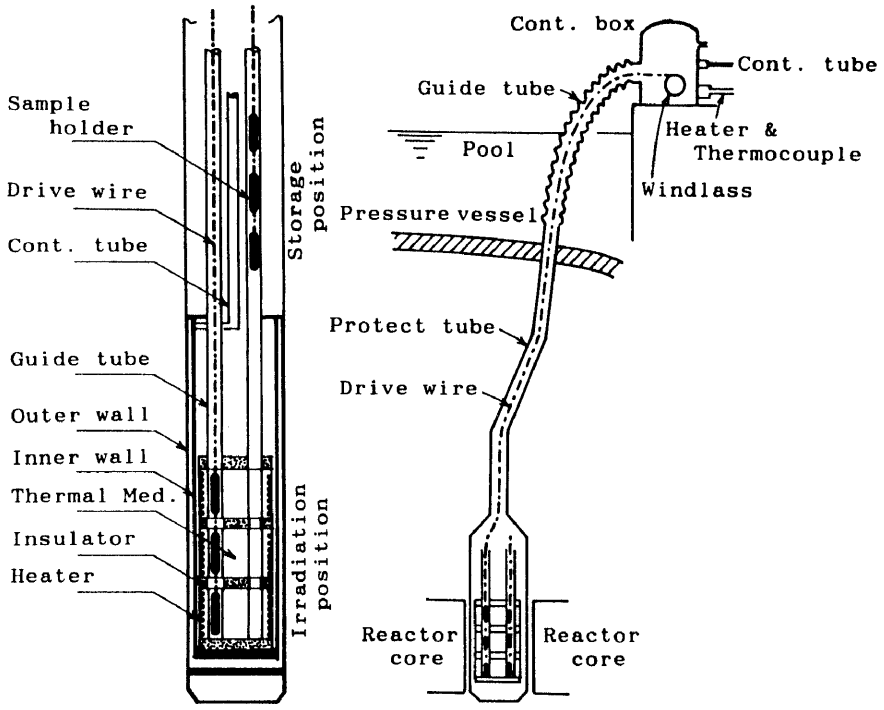

Fig. 35. Multi-section multi-division irradiation rig for controlled irradiation in JMTR under design and test.

However, the instability of small loops can be certainly one of the major reason of the very small success probability of the formation of interstitial type dislocation loops from collision cascades.

At the end of this section, a method is proposed to improve the currently poor situation of fission-reactor neutron irradiation into a systematic and reliable experiment. In order to perform long and short irradiations with a fission reactor under consistent improved control, a newly designed irradiation rig is being constructed which enables us to remove part of samples during reactor operation without losing the temperature control as shown in Fig. 35. It is called the Multi-Section Multi-Division Controlled Irradiation Capsule and will be used in JMTR.

14. Development of Controlled Temperature-Cycle Irradiation Technique in JMTR[5)]

To investigate the effect of cyclic temperature change during neutron irradiation upon radiation induced microstructure evolution and resulting property changes of materials is very important from both fundamental and engineering viewpoints. Therefore, a technique that allows us to do the controlled temperature-cycle irradiation wa;s developed;d in the Japan Materials Testing Reactor (JMTR). The technique meets the following requirements: (1) the temperature-cycle irradiation is to be performed under three different condition by changing lower and upper temperatures; 200°C<-->400°C, 300°C<-->400°C and 300°C<-->450°C. (2) the number and period of the temperature-cycles are to be six for 24-days full irradiation and approximately 44 h/44 h at the lower/upper temperatures. (3) the temperatures of each specimen assembly are to be maintained at the lower temperatures before start-up of the reactor and at the upper temperatures during shut-down until the complete absence of reactor power. In this paper, the details of the irradiation rig, successful results and several problems to be overcome for future improvement are presented.

15. Microstructure Evolution by Neutron Irradiation during Cyclic Temperature Variation[24)]

Utilizing the technique to control the temperature being not influenced by the operation mode of a reactor, an irradiation during which the temperature was alternatively changed several times between two temperatures (T-cycle) is performed. Three temperature combinations were 473K/673K, 573K/673K and 573K/723K. Fig. 36 shows the recorded temperature history for half of the reactor operation cycle. The total neutron irradiation dose were 0.8×10^{24}n/m^2, 1.4×10^{24}n/m^2 and 1.2×10^{24}n/m^2, respectively for the three combinations.

Some defect structures are understood by the combination of the defect processes in lower and higher

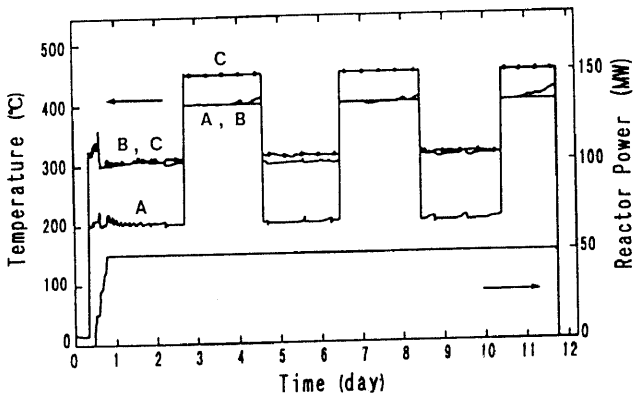

Fig. 36. Recorded history of temperature during T-cycle irradiation. This is the half of a cycle and irradiation was done again with the identical temperature history.

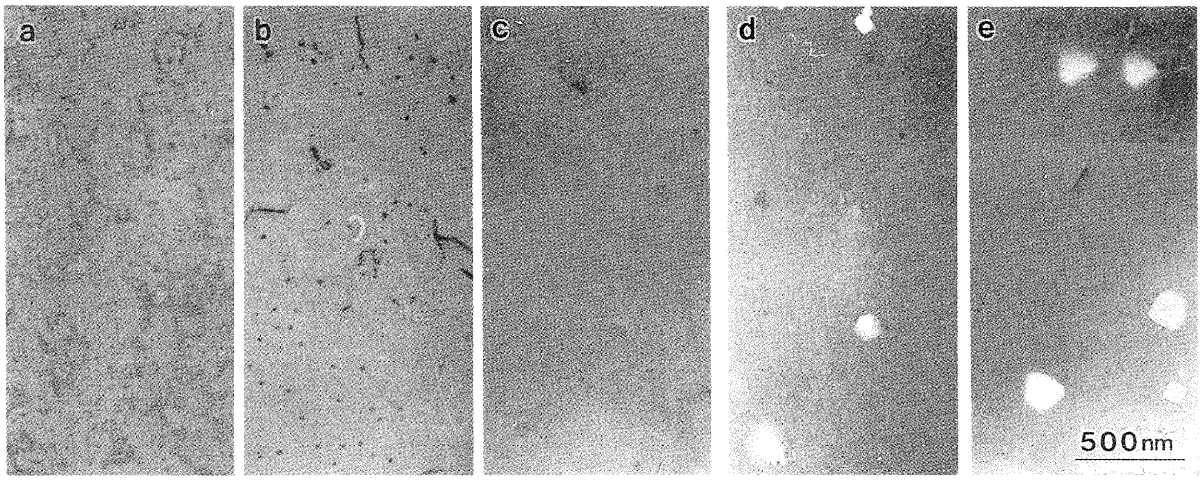

Fig. 37. Defect structures developed in copper by two T-cycle irradiations. (d) 473K/673K, $8.3x10^{23}n/m^2$ and (e) 573K/673K, $1.4x10^{24}/m^2$. And those by constant temperature irradiation at three related temperatures. (a) 473 K, $2.5x10^{23}/m^2$, (b) 573 K, $3.7x10^{23}/m^2$ and (c) 673 K, $9.6x10^{23}/m^2$,

temperatures, and some others are understood if the defect processes during the transient between the two temperatures is taken into consideration.

A clear example in copper is shown in Fig. 37 in which the defects characteristic of the temperatures between the two in T-cycle irradiation. Voids are formed in copper at a narrow range of temperature at around 573 K. In the T-cycle irradiation of 473K/673K, voids are thought to have nucleated when the temperature passed through 573 K.

The most remarkable characteristic of the T-cycle irradiation is in the remarkably different microstructures than those expected from the simple combination of the two temperatures including the temperatures between the two. As shown in an example of Fig. 38, the defect microstructures in T-cycle irradiation is much less than expected from all the temperatures involved.

During the irradiation at the lower temperature of T-cycle irradiation of Ni, Cu and 316SUS-M, both types point defect clusters, vacancy and interstitial, are continuously accumulated. Although the vacancy clusters directly produced from cascade collisions are continuously annihilated during irradiation, there still high density remains as shown in Fig. 39. At the lower temperature 473 K, the amount of vacancies in their clusters is several times more than the amount of interstitials in their clusters for all three materials. At the higher temperature 573 K, vacancies are not less than interstitials, though the difference is not remarkable.

Vacancies evaporated from the vacancy clusters at higher temperature can eliminate interstitial clusters completely as shown schematically in Fig. 40, and the repetition of these processes leads to unexpectedly slow defect structure development by T-cycle irradiation.

16. Role of Solute Atoms on Microstructural Evolution in Neutron Irradiated Nickel[25]

Fission reactor irradiation of nickel alloys with solutes of widely varied volume size factors, 2 at.% of Si, Cu, Ge and Sn, was performed for a wide range of irradiation temperature. All the irradiations were performed with improved temperature control which is not influenced by

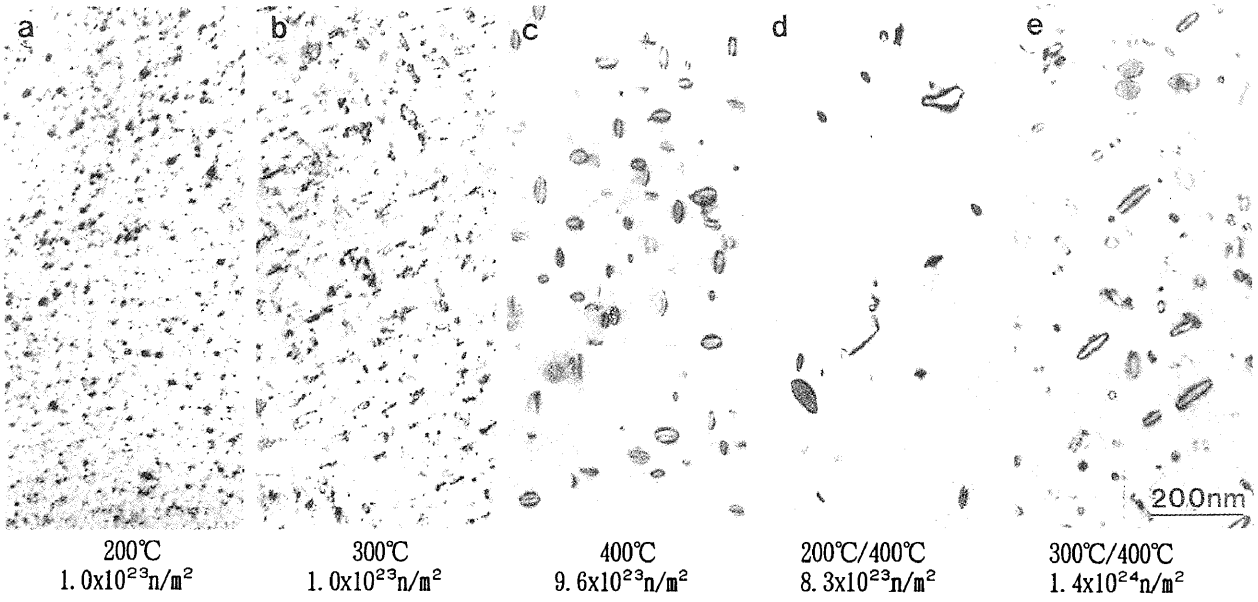

Fig. 38. Defect structures developed in 316SUS-M by two T-cycle irradiations. Irradiation conditions for (a)-(d) are same as in Fig. 38, respectively.

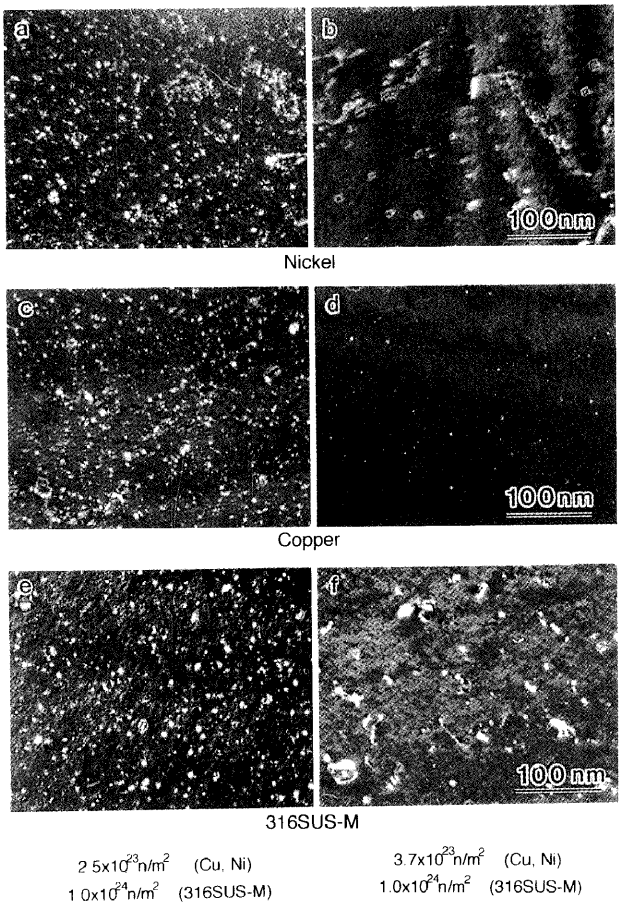

Fig. 39. Small point defect clusters accumulated in three materials, (a) and (b) Ni, (c) and (d) Cu, and (e) and (f) 316SUS-M, at the lower temperature of the combination in T-cycle irradiation. 473 K irradiation on the left and 573 K irradiation on the right.

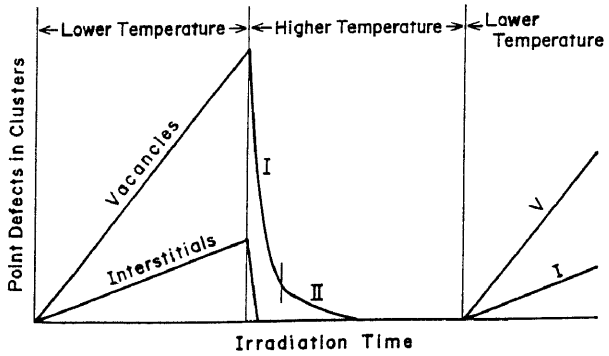

Fig. 40. Schematic illustration of the accumulation of point defect clusters during lower temperature irradiation and the annihilation during higher temperature irradiation.

the reactor power.

At a lower temperature 473 K, high density of small vacancy clusters are mixed with interstitial type dislocation loops in all the alloys as shown in Figs. 41 and 42.

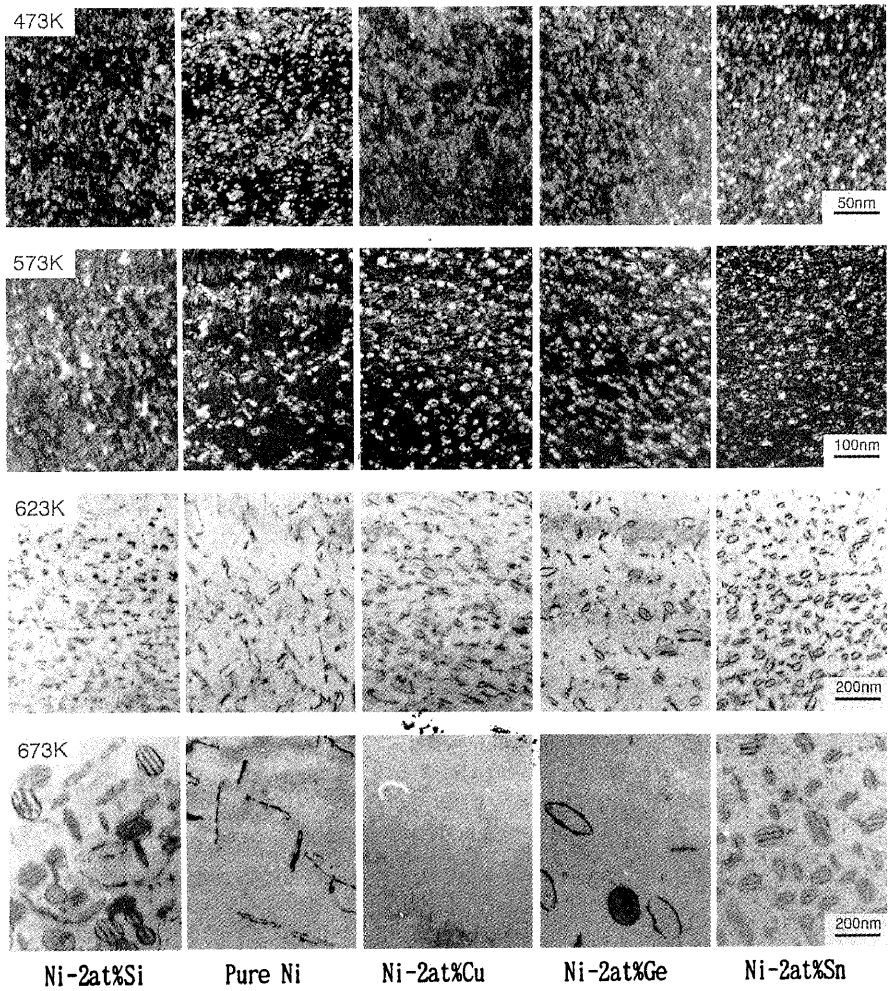

Fig. 41. Defect structures introduced in specimens irradiated as thin foils, at 473 K ($2.5x10^{23}/m^2$), 573 K ($3.7x10^{23}n/m^2$) and 673 K ($9.6x10^{23}n/m^2$).

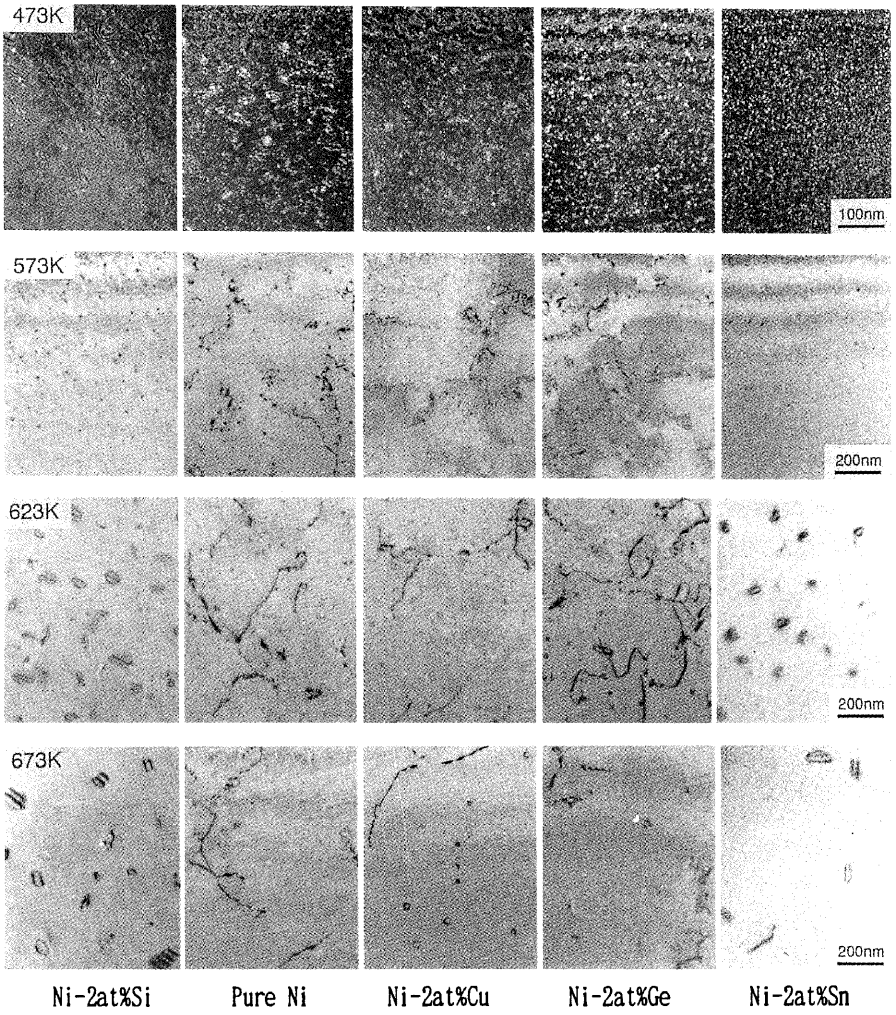

Fig. 42. Defect structures introduced in specimens irradiated as bulk, at 473 K ($2.5x10^{23}/m^2$), 573 K ($3.7x10^{23}n/m^2$) and 673 K ($9.6x10^{23}n/m^2$).

At higher temperatures, in the alloys with solutes of negative volume size factor Si and extremely large positive factor Sn, interstitial type dislocation loops remain as faulted during their growth as in the figures. Solutes in these alloys are playing an important role in preventing the unfaluting of faulted interstitial loops. Staying faulted, the loops grow only with a moderate speed with small bias to absorb interstitials. In addition, the faulted loops are positionally stable and cannot join to other loops by changing their position. This again prevents the rapid development of dislocation structure.

during irradiation In the alloys with solutes of positive but not large volume size f actor Cu and Ge including pure Ni, unfaluting of loops strongly promote the development of dislocation structures. As a consequence of the difference in these dislocation structure development, void formation is almost completely suppressed in the first category, and it is enhanced strongly in the second.

17. Microstructural Evolution in Low Dose Neutron Irradiated Fe-15Ni-15Cr Alloy[26]

Reactor irradiation of the base alloy of modified austenitic stainless steel Fe-15Ni-15Cr, the candidate alloy for fusion reactor application, was performed with improved temperature control.

All the three types of defects, vacancy clusters in the form of stacking fault tetrahedra, interstitial type dislocation loops and voids, are more pronounced in samples irradiated with conventional temperature control than those with improved control. Fig. 43 shows an example of the comparison. They are attributed to the nucleation of those

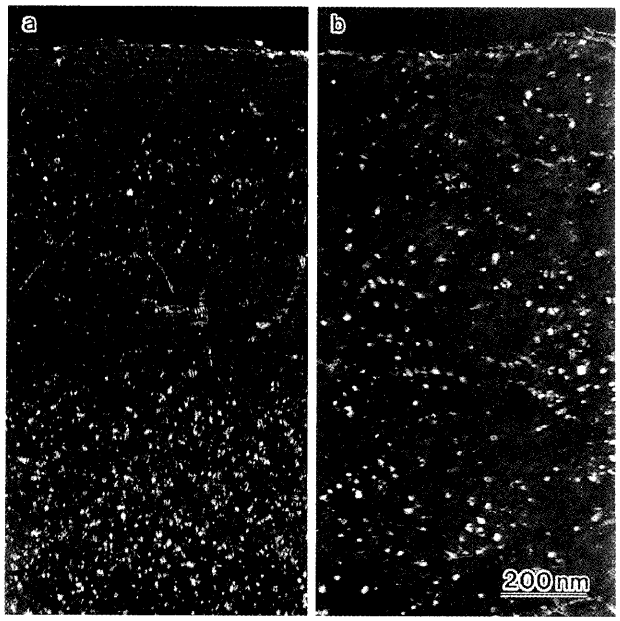

Fig. 43. Complex variation of defect structures with specimen thickness in a thin foil irradiated with (a) conventional temperature control and (b) was irradiated with improved control. Irradiation at 473 K up to $1x10^{24}n/m^2$.

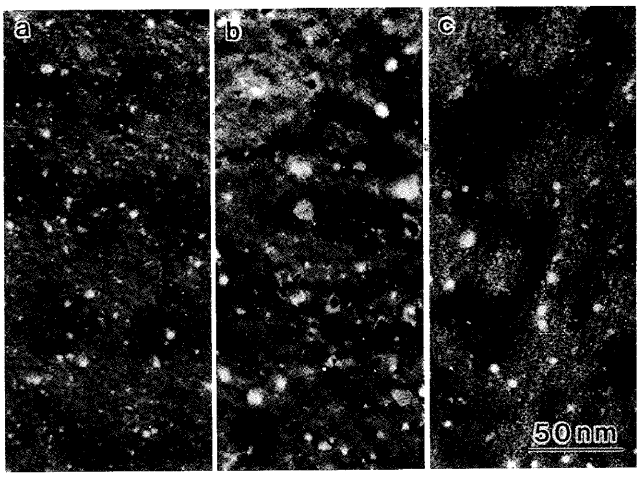

Fig. 44. Point defect clusters formed at thin parts of thin foils at three temperatures. (a) 373 K, (b) 473 K and (c) 573 K, all up to 1.1×10^{24}n/m^2.

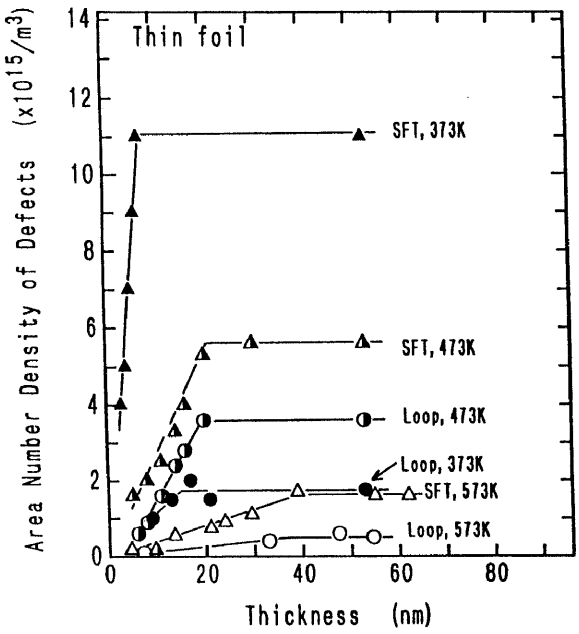

Fig. 45. Variation of area number density of point defect clusters with specimen thickness in specimens irradiated as thin foils.

defects during the start-up of the reactor.

From the irradiation of thin foils, the role of freely migrating interstitials was extracted. Fig. 44 shows the defects produced in thin foils at three temperatures, observed with weak beam dark field technique. As shown in Fig. 45, area number density of both stacking fault tetrahedra (SFT) and dislocation loops increased with specimen foil thickness and they level off at thicker area. In the thin part of specimen for which the defect number density increases proportionally to the foil thickness, point defect clusters produced by cascades, especially SFT, can be regarded not influenced by freely migrating point defects. At the thicker part, number of point defect clusters increases no more with the increase of thickness, because of the annihilation by freely migrating point defects deep inside the foil.

For bulk irradiation, the variations of three types of defects above mentioned with irradiation temperature are thoroughly investigated. Fig. 46 shows defect structures introduced in bulk samples at five temperatures, 373, 473, 573, 623 and 673 K. At 373 K and 473 K, they are mixture of high density of small SFT and dislocation loops. At 573 K, appreciable size of dislocation loops are mixed with small SFT, and some scattered small voids are observed. At 673 K and above, well developed loops with stacking fault are observed but no SFT. Number of voids decreases with the increase of temperature but the size increases.

All the experimental observation and their analysis showed that the reaction of freely migrating point defects in SUS is less than in pure metals.

18. Effect of Cascade Localization Induced Bias Effect and Fluctuation of Point Defect Reactions on Defect Structure Evolution near Planar Sinks

Defect structure developments near planar sinks are analyzed as a competition of two effects. One is the cascade localization induced bias (CLIB) effect which leads vacancy dominant point defect reactions during cascade damages. The

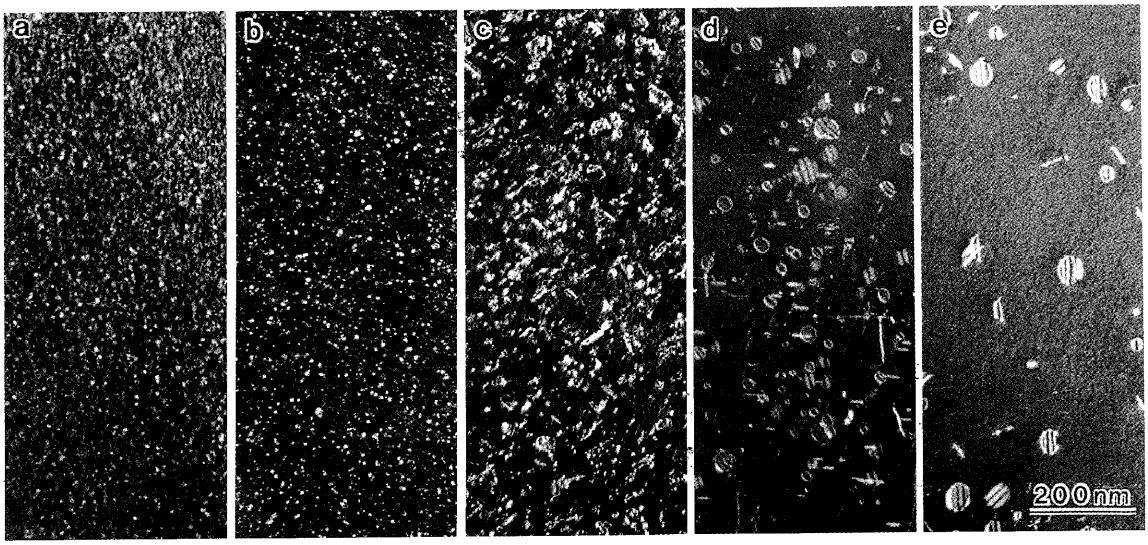

Fig. 46. Defect structures introduced in specimens irradiated as bulk at five temperatures.

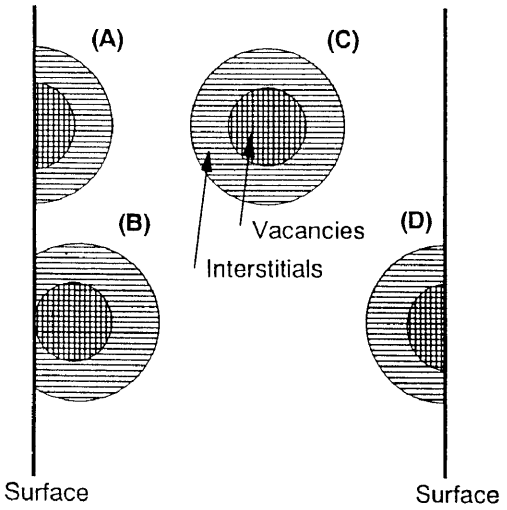

Fig. 47. Schmatic illustration of four cases of cascade damages in relaltion to surfaces.

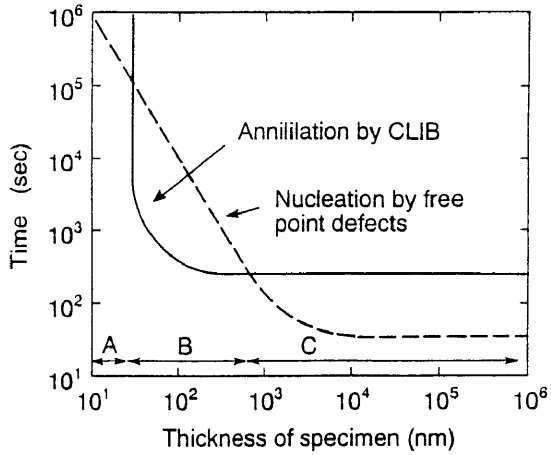

Fig. 48. Annihilation time by the CLIB effect and nucleation time by freely migrating point defects. Three areas A, B and C are explained in Fig. 47.

other is a stochastic fluctuation effect of point defect reactions between defect clusters and freely migrating point defects. The sink geometry plays an important role for these effects, and Fig. 47 show the cases analyzed in which the relation of the cascade with the planer sinks is illustrated.

The strength of two effects as a function of the distance to planar sinks is analyzed as shown in Fig. 47. The comparison is made between the analysis and experimental results. In a thin specimen only small cascades are formed and the CLIB effect does not work effectively. With increasing the thickness, large cascades begin to contribute to the CLIB effect.

As shown in Fig. 48, at the very thin part of specimen (area A in Fig. 48), though a long time is required before the nucleation of loops owing to the low concentration of point defects, embryos, small interstitial clusters formed by cascade damages can nucleate to loops because of no annihilation by the CLIB effect. At the intermediate thickness of a specimen (area B in Fig. 48), the concentrations of point defects increase, which leads shorter nucleation time of loops. Before the annihilation of embryos by the CLIB effect, they can absorb enough point defects and nucleate to loops.

References

1) M. Kiritani, N. Yoshida and S. Ishino: J. Nucl. Mater. 122 & 123 (1984)602.
2) M. Kiritani: J. Nucl. Mater. 160 (1988) 135.
3) M. Kiritani, T. Yoshiie, S. Kojima, Y. Satoh and K. Hamade, J. Nucl. Mater. 174 (1990) 327.
4) F. A. Garner, N. Sekimura, M. L. Grossbeck, A. M. Ermi, J. W. Newkirk, H. Watanabe and M. Kiritani: J. Nuc. Mater. 205 (1993) 206.
5) M. Narui, H. Kurishita, H. Kayano, T. Sagawa, N. Yoshida and M. Kiritani: J. Nucl. Mater. (1994) in press.
6) M. Kiritani: J. Nucl. Mater. 200 (1993) 156.
7) M. Kiritani: J. Nucl. Mater. 133 & 134 (1985) 85.
8) M. Kiritani, T. Yoshiie and S. Kojima: J. Nucl. Mater. 141-143 (1986) 626.
9) M. Kiritani: J. Nucl. Mater. 1550157 (1988) 113.
10) M. Kiritani: J. Nucl. Mater. 179-181 (1991) 81.
11) M. Kiritani: J. Nucl. Mater. 191-194 (1992) 125.
12) M. Kiritani: Ultramicroscopy 39 (1991) 135.
13) M. Kiritani, M. Hoshino, H. Kato, H. Matsui and N. Matsunami: J. Nucl. Mater. 191-194 (1992) 1128.
14) M. Kiritani, Y. Fukuda, T. Mima, E. Iiyoshi, Y. Kizuka, S. Kojima and N. Matsunami: J. Nucl. Mater. (1994) in press.
15) M. Kiritani: Mater. Sci. Forum 97-99 (1992) 141.
16) T. Yoshiie and M. Kiritani: Mater. Sci. Forum 97-99 (1992) 105.
17) T. Yoshiie and M. Kiritani: J. Nucl. Mater. 191-194 (1992) 1088.
18) S. Kojima, T. Yoshiie, K. Hamada and M. Kiritani: J. Nucl. Mater. 191-194 (1992) 1155.
19) Y. Satoh, T. Yoshiie and M. Kiritani: J. Nucl. Mater. 191-194 (1992) 1101.
20) T. Yoshiie, S. Kojima, Y. Satoh, K. Hamada and M. Kiritani: J. Nucl. Mater. 191-194 (1992) 1160.
21) N. Yoshida, Q. Xu, H. Watanabe, T. Muroga and M. Kiritani: J. Nucl. Mater. 191-194 (1992) 1114.
22) T. Yoshiie, K. Hamada, S. Kojima and M. Kiritani: Defect and Diffusion Forum 95-98 (1993) 243.
23) M. Kiritani, T. Yoshiie, S. Kojima and Y. Satoh: J. Nucl. Mater. 205 (1993) 460.
24) M. Kiritani, T. Yoshiie, M. Iseki, S. Kojima, K. Hamada, M. Horiki, Y. Kizuka, H. Inoue, T. Tada and Y.Ogasawara: J. Nucl. Mater. (1994) in press.
25) K. Hamada, S. Kojima, Y. Ogasawara, T. Yoshiie and M. Kiritani: J. Nucl. Mater. (1994) in press.
26) M. Horiki and M. Kiritani: J. Nucl. Mater. (1994) in press.
27) T. Yoshiie and M. Kiritani: J. Nucl. Mater. (1994).